Journal of Power Sources 264 (2014) 49–58

Contents lists available at ScienceDirect

Journal of Power Sources

journal homepage: www.elsevier.com/locate/jpowsour

Development and testing of an economic grid-scale flow-assisted zinc/nickel-hydroxide alkaline battery

Damon E. Turney [a,*], Michael Shmukler [b], Kevin Galloway [b], Martin Klein [c], Yasumasa Ito [d], Tal Sholklapper [e], Joshua W. Gallaway [a], Michael Nyce [a], Sanjoy Banerjee [a]

[a] The City University of New York, Energy Institute, Department of Chemical Engineering, USA
[b] Urban Electric Power Corporation, USA
[c] None, Retired
[d] University of Nagoya, Department of Mechanical Engineering, Japan
[e] Voltaiq Corporation, USA

HIGHLIGHTS

- We present a new design of nickel zinc battery at bench scale and grid scale.
- We present cycle testing, failure analysis and gas sealing of this new battery.
- Zinc particulates and nickel surface passivation are the primary failure mechanisms.
- Cycle life of over 3000 is achieved and cost estimates show low cost, $407 per kWh.

ARTICLE INFO

Article history:
Received 2 February 2014
Received in revised form
11 April 2014
Accepted 14 April 2014
Available online 26 April 2014

Keywords:
Battery testing
Alkaline
Grid-scale
Zinc morphology

ABSTRACT

An economic design for an alkaline zinc-anode flow-assisted battery without membrane separators was tested at grid-scale of 25 kWh with a string of thirty 833 Wh cells in series, and also at bench scale with individual 28 Wh cells. The bench-scale tests allowed optimization of parameters such as electrolyte flow, choice of hardware material, electrolyte composition, and charge/discharge protocol. The best-performing bench scale cell cycled for over 3300 cycles with energy efficiency above 80%, and was selected as the design basis for scale-up to the 25 kWh battery string. Testing of the grid-scale string demonstrated 1000+ cycles with round trip energy efficiency above 80%. Two challenges observed at the bench scale were overcome for successful scale-up, namely a) passivation of the anode surface, which occurred when the anode experienced voltages 100 mV above zinc's rest voltage, and b) zinc particulates that jammed the gap between the electrodes and caused cathode degradation and passivation of the anode surface. Best practices to overcome these challenges and achieve long cycle life are presented.

1. Introduction

Electrical energy storage at MWh scale is under widespread development as a means to improve grid stability in the increasingly sophisticated electric power market. The leading motivation for energy storage is growth of solar and wind power, which at grid-penetration above ~20% requires energy storage to smooth out variability [1,2]. Other applications with significant demand for energy storage are nighttime load shifting, demand-charge reduction and uninterruptible power supply applications. Market analysis typically suggests target costs for the grid-scale battery system to be less than $500 per kWh, with cycle life above 2000 and discharge capability that allows total capacity to be delivered in less than two hours [3–6]. These performance numbers mean new battery technology will have to be developed. Existing lead-acid batteries are unlikely to be suitable because they cannot discharge their capacity in less than three hours without significant loss of capacity or cycle life. Widespread manufacturing and use of lead is also undesirable due to environmental concerns. Existing nickel–zinc batteries are limited by the early failure of the pasted zinc anode, after ~700 cycles [15], which causes the cost per life-time kWh-delivered to be too high. Fire safety is also likely to play a

* Corresponding author. 160 Convent Ave., CCNY, ST316, New York, NY 10031, USA.
E-mail addresses: damonturney@gmail.com, dturney@ccny.cuny.edu (D.E. Turney).

http://dx.doi.org/10.1016/j.jpowsour.2014.04.067
0378-7753/

role. In residential or urban locations the fire risks of the batteries are required to be very low, and relatively high fire risk exists for lithium ion, molten-metal, or sodium sulfur technologies. To work toward meeting the market requirements, this paper reports further development of flow-assisted alkaline batteries with zinc anodes and sintered-nickel nickel-hydroxide cathodes [7,8], based on the reactions

$$\text{cathode}: \quad 2NiOOH + 2H_2O + 2e^- \Leftrightarrow 2Ni(OH)_2 + 2OH^- \qquad (1)$$

$$\text{anode}: \quad Zn + 4OH^- \Leftrightarrow Zn(OH)_4^{2-} + 2e^- \qquad (2)$$

in 9 M KOH electrolyte, which meet the performance goals and have negligible risk from fire or chemical hazard. Our "flow-assist" battery is not the same as a flow battery, but simply means that the electrolyte is circulated inside each cell, through flow gaps between the electrodes, to improve the electrodeposition and dissolution of zinc during long-term cycling.

We have conducted and published results of previous experiments [7,8] with the same basic technology and demonstrated cycle life up to 1500 in 3.7 Ah cells. These results indicated that the coulombic efficiency and discharge capacity were improved if electrolyte flow velocity was increased above 10 cm s^{-1}. The pumping costs are significant at these flow-assist velocities therefore we choose flow rates of 0.5–1 cm s^{-1} which are shown in Subsection 3.3 to require only 4% of the energy stored in the battery cell.

2. Experimental

2.1. Bench-scale cell testing

Bench scale tests were conducted with 19 Ah (31 Wh) cells of specifications shown in Table 1. The goal of the bench scale tests was to optimize design of the larger grid-scale cells that would comprise the 25 kWh battery. Fig. 1 shows CAD drawings of a bench scale cell. A polysulfone box of 1.5 L volume (outside dimensions) contained the electrolyte and electrodes. The electrode plates stood upright, parallel to each other, with cathode plates separated from anode plates by a 3 mm gap of upward-flowing electrolyte created with 3 mm diameter PMMA dowel rods spaced apart by 15 mm. The electrode plates were sealed inside a PMMA "chimney" box (i.e. with an open top) that was immersed in the electrolyte. The two tube ports seen on the top lid allowed electrolyte to be pumped into the bottom of this chimney box, causing the electrolyte to flow upward between the electrode plates, as shown with the arrows of the right side drawing of the figure. At the top of these channels the flow was restricted by a narrow gap, which homogenized the flow of electrolyte to be the same velocity in each channel. The electrolyte then spilled out the top of the chimney and then circulated through the pump again. Table 1 specifies the baseline design of these bench-scale cells (19 Ah, 28 Wh). The sintered-nickel cathodes were obtained from Jiangsu Highstar Battery Company. The nickel-plated anodes were obtained from Orbel Corporation. All other chemicals were obtained from Fischer Scientific or Sigma Aldrich, and all other hardware from McMaster Carr. Nuts, bolts and hardware were electroless nickel plated.

Table 1
Bench scale cell design (baseline design).

Design parameter	Value
Electrolyte volume	0.95 L
Electrode size	10 × 9 cm, with some regions masked
Number of anodes	9
Number of cathodes	8
Gap between electrodes	3 mm
Cathode material	0.66 mm Highstar sintered nickel cathode
Cathode discharge capacity	0.03 Ah cm^{-2}, total for cell is 19 Ah
Anode material	0.14 mm copper sheet coated with 5 μm of nickel
Anode electro-deposition capacity	60 g L^{-1} of ZnO in 0.95 L equates to 38 Ah
Zincate concentration in electrolyte	60 g ZnO L^{-1}
Potassium hydroxide concentration in electrolyte	45% w/w
Energy density	20.9 Wh L^{-1}
Specific Energy	17.3 Wh kg^{-1}
Flow velocity upward between electrode plates	0.5 cm s^{-1}
Material of bolts, tabs, hardware	Nickel coated steel or nickel coated copper

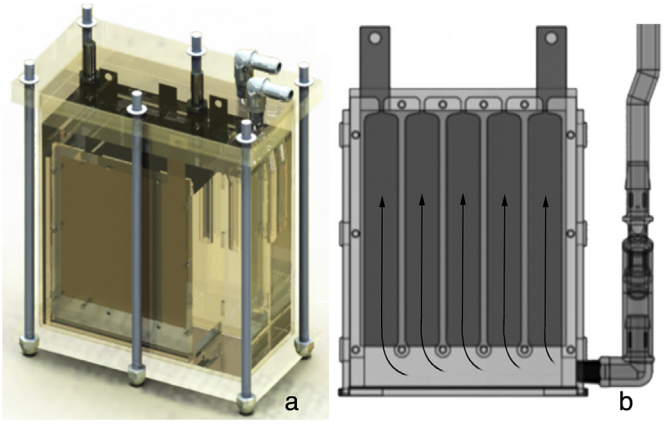

Fig. 1. a) The bench-scale cell is shown. b) A cross-section of the "chimney" box that was immersed in the electrolyte is shown, where the electrodes are dark grey and PMMA dowel rods are light grey.

The open-circuit voltage of the bench and grid scale cells ranged from 1.50 V at low state-of-charge to 1.80 V at high state-of-charge. This change in cell voltage was due to the nickel hydroxide cathode [9]. The voltage of the zinc anode remained always within 20 mV of zinc's reference voltage in the same electrolyte. Cycling was performed at 100% depth of discharge with an Arbin Instruments BT-2000 battery tester. The cycling protocol charged the cells at a constant current rate of "full capacity in two hours" (9.5 A). The charging switched to constant voltage at 1.93 V, to avoid excessive gassing of oxygen. Discharge of the cells was also performed at constant current "full capacity in two hours" (−9.5 A), ending when the cell voltage dropped below 1.2 V. These charge/discharge rates allowed roughly five cycles to be tested per day. The upward flow velocity of electrolyte between the electrode plates was ensured to be 0.5 cm s^{-1}. As described in Ref. [8] the cells were put through an "anode cleaning" every 10th cycle to remove excess zinc off the anodes. The anode cleaning procedure discharged the cells at constant current "full capacity in ten hours" (−2.0 A) until the cell voltage reached −0.1 V, after every tenth cycle. This cleaning discharge current of −2.0 A was found to be too high for optimal performance, but a full description of this is left for Subsection 3.1. A list of our bench scale tests and results is given in Table 2 in Section 3.1.

2.2. Gas sealing the cell, and maintaining proper electrode state-of-charge

Metallic zinc is well known to experience a corrosion reaction with the electrolyte that slowly dissolves the zinc and produces gaseous bubbles of hydrogen [10,12,13]. The anode's nickel surface

Table 2
Grid-scale 555 Ah cell design.

Design parameter	Value
Electrolyte volume	25 L
Electrode size	36 × 15 cm, with some regions masked
Number of anodes	40
Number of cathodes	39
Cathode material	Sintered nickel impregnated with nickel hydroxide
Cathode capacity	0.03 Ah cm^{-2} for a total of 833 Wh
Anode material	Copper sheet coated with 5 μm of nickel
Anode capacity	60 g L^{-1} of ZnO in 24 L equates to 1976 Ah
Zincate concentration in electrolyte	60 g ZnO per L
Potassium hydroxide concentration in electrolyte	37% w/w
Energy density	15.6 Wh kg^{-1} and 19.6 Wh L^{-1}
Electrolyte velocity between electrode plates	0.5 cm s^{-1}
Material of bolts, tabs, hardware	Nickel coated steel or nickel coated copper

also generates hydrogen gas by electrolysis of the electrolyte. The cathode generates oxygen gas during charge. Gas generation in batteries is a serious practical concern, and has prompted research describing the process in detail [7]. Industrial operation, lead-acid as a prime example, requires fire safety such that all gas releases are well below the lower explosive limit for any flammable gas content [12]. Placing a platinum catalyst recombiner in the gas headspace of the battery is common practice to accomplish recombination of hydrogen and oxygen gas. In this subsection we describe a method that gives two benefits, the first being optimal performance of the recombiner to allow sealing of the battery, and the second being quantitative tracking of the state of charge of the anode with respect to the cathode [14].

The significant reactions that occur on the anode are

$$\text{undesired}: \quad 2H_2O + 2e^- \Leftrightarrow H_2(g) + 2OH^- \tag{3}$$

$$\text{desired}: \quad Zn\left(OH^-\right)_4^{2-} + 2e^- \Leftrightarrow Zn(\text{metallic}) + 4OH^- \tag{4}$$

and the significant reactions that occur on the cathode are

$$\text{undesired}: \quad 4OH^- \Leftrightarrow O_2(g) + 2H_2O + 4e^- \tag{5}$$

$$\text{desired}: \quad Ni(OH)_2 + OH^- \Leftrightarrow NiOOH + H_2O + e^- \tag{6}$$

therefore if the amount of gas created by the cathode and anode are known, the "lost" coulombs of state-of-charge can be calculated for each electrode. Four electrons are required to create an O_2 gas molecule, and two electrons are required for a H_2 gas molecule. The difference in state-of-charge between the cathode and anode, in units of coulombs, is calculated as

$$\Delta SOC = FV(4[O_2(g)] - 2[H_2(g)]) \tag{7}$$

where F is Faraday's constant, V is the volume of the cell's headspace, $[O_2(g)]$ is the oxygen concentration and $[H_2(g)]$ is the hydrogen concentration in the cell's headspace, e.g. in units of moles per liter.

The gas recombiner in the battery headspace eliminates oxygen and hydrogen molecules according to the equation

$$2H_2(g) + O_2(g) \rightarrow 2H_2O, \tag{8}$$

where it is seen that two oxygen molecules are eliminated for every one hydrogen molecule eliminated, consequently ΔSOC is unaffected by the operation of the recombiner.

Attaching simple gas pressure sensors and hydrogen (or oxygen) partial pressure sensors to the headspace provides the input needed to calculate the above chemical equations, which in turn allows quantitative knowledge of the state-of-charge of the cathode with respect to anode. Due to zinc corrosion, it is common for the anode's state-of-charge to progressively become less than that of the cathode, the symptom of which is excess hydrogen in the headspace. The catalytic recombiner eliminates hydrogen only when oxygen is present, therefore if the cathode's state-of-charge is too far out of balance with the anode the recombiner cannot operate, and pressure builds up in the head space. In this situation a sheet of nickel foam becomes useful because it may be connected to either the cathode or the anode to catalytically enhance the gas production at either electrode, by principle of Eq. (3) or Eq. (5). For example, the nickel foam may be connected to the cathode during charging to generate additional oxygen gas to allow Eq. (8) to proceed, or alternatively it may be connected to the anode to generate extra hydrogen gas. In this way the balance of gases in the headspace may be controlled to be stoichiometric for Eq. (8) to work optimally. This gas control system [14] was built into a prototype 19 Ah cell using an Arduino logic controller and readily available transistors for making the electrical connection from the nickel foam to the desired electrode. The cell was initially filled with pure oxygen and tightly gas-sealed from the environment. No gas was allowed to escape or enter. A pressure sensor manufactured by SSI Technologies, model P51, and an oxygen sensor made by Apogee Instruments, model SO, gave the measurements necessary to calculate oxygen and hydrogen gas partial pressures. Results are given in Sections 3.1 and 3.2.

2.3. Grid scale battery testing

We settled on the 555 Ah cell design shown in Fig. 2a), with specifications shown in Table 2. Thirty-five of these large 833 Wh cells were built, and thirty of them were strung together to form the 25 kWh battery shown in Fig. 2b). Voltages across the battery ranged from 40 to 60 V, depending on state of charge. An Arbin Instruments battery tester (capable of 300 A and 300 V) was used for cycling of the battery at 100% depth-of-discharge. The voltage on each cell of the battery was monitored by a series of slave digital processors communicating wirelessly with a master digital processor. Balancing of the cells was managed by automated bleeding of all cells through 0.15 Ohm resistors, one per cell. This balancing algorithm bled all cells with voltage above that of the lowest two cell-voltages. The bleeding occurred only during the last half of the discharge step.

The charging and discharging procedures used for the grid-scale battery were the best practices learned from the bench scale tests, wherein charging and discharging both occurred at "full capacity in two hours" (278 A on charge and −278 A on discharge). To maximize charging, a secondary charge step of lower current (100 A) put the final charge into the battery. An anode-reconditioning step was also used in between every tenth cycle, to clean excessive zinc off the anode plates and avoid short-circuiting. This anode reconditioning occurred at −20 A. All gas emission from the batteries were routed through catalytic converters to eliminate hydrogen. These catalysts are seen in Fig. 2b) as the metallic egg shaped objects. Hydrogen sensors were installed in the test room, however hydrogen was never detected during the testing.

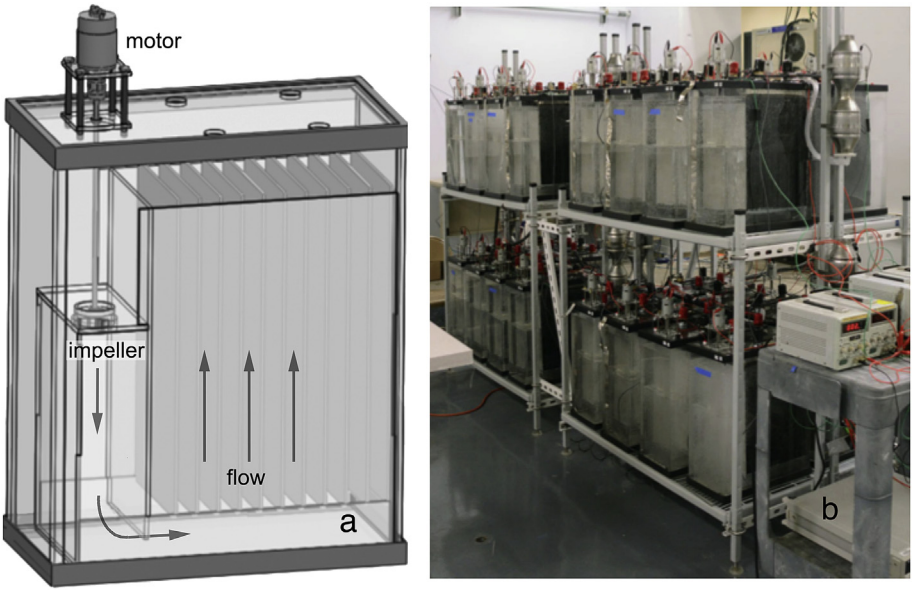

Fig. 2. a) A CAD drawing of the 555 Ah cell, where only every eighth electrode plate is shown, and a motor is shown coupled to an impeller that keeps electrolyte flowing upward between the electrodes at ~0.5 cm s^{-1}. b) A photograph of the completed grid-scale 25 kWh battery.

3. Results and discussion

3.1. Bench scale performance and failure mechanisms

With the 19 Ah bench scale cells described in Subsection 2.1 we tested the following perturbations to the baseline design: flow homogeneity, potassium hydroxide concentration, zincate concentration, stainless steel hardware vs. nickel hardware (terminals, tab collectors, bolts, nuts), cycling protocol, and graphite-paste nickel-hydroxide cathode instead of sintered nickel cathode, all shown in Table 3. A special design test is shown in the last row of Table 3, where as described in Subsection 2.2 a nickel foam sheet was placed into the electrolyte to be used when-needed as a substitute for the anode or cathode [14].

The 3300 cycle life of our best performer, shown in Fig. 3, is verification of the longevity possible of this technology. The shape change problem that typically limit pasted zinc anodes to ~500 cycles is clearly not an issue with our cells [12]. With further research it is clear that nameplate cycle life of 5000 is achievable. Discharge rate testing of the technology was performed on a cell that had half the number of cathodes and anodes, giving a cell capacity of 8.5 Ah. The results of discharge rate testing are shown in Fig. 4, where it is seen that a 1-h discharge rate did not significantly decrease the discharge capacity of the battery cell. An even faster discharge rate of 0.5-h gave 7.9 Ah of capacity, as compared to 8.5 Ah at a slow discharge rate of 2-h. This high-rate performance is favorable when compared to traditional lead-acid batteries which lose ~50% of their capacity at a 1-h discharge rate.

Table 3
Performance results of 19 Ah bench scale cells (100% capacity testing).

Cell ID	Perturbation from baseline design	Cycle life
37KOH 60ZnO	37% KOH	3300
37KOH 40ZnO	37% KOH, 40 g L^{-1} zincate	553
45KOH 40ZnO	40 g L^{-1} zincate	691
Ni Restricted	baseline	1132
Ni Unrestricted	No flow homogenizers	620
18-8 Restricted	Stainless steel components	1451
18-8 Unrestricted	Stainless steel components, no flow homogenizers	672
Paste teflon-bound	Paste cathode instead of sintered nickel cathode	789
Balancing cell	Nickel foam sheet used to balance gasses	1310

As mentioned above, during testing of the bench scale cells we made many discoveries regarding to the best practices for the cycling procedure. During the first few hundred cycles we observed by visual inspection of the flow channels that zinc particulates were falling off the anodes during the anode cleaning step and clogging the flow gap between the electrodes during their decent to the bottom, causing short circuits and decreasing cell efficiency and capacity. As a solution to this problem, the discharge current during the anode cleaning step was reduced to “cell capacity in thirty hours” (−0.6 A). This lower current, compared to our baseline method of using −2.0 A, decreased the rate of particulates falling off, and eliminated the clogging and short-circuiting problem.

A second problem seen in the first few hundred cycles occurred during charging, wherein electrodeposition of zinc onto the anode would fail. Instead of zinc electrodeposition, hydrogen gas would bubble at the anode surface due to electrolysis of the electrolyte, causing the discharge capacity of the anode to be significantly reduced (sometimes as low as 25% of nominal). The cause of this “passivation” of the anode surface, i.e. poor electrodeposition charge efficiency, was unknown, but was important because it lead to several problems. The first discharge after a poor electrodeposition event leaves the cathode with much higher state of charge compared to the anode. Therefore, in the subsequent charging step, the cathode is overcharged and large volume expansion of the nickel hydroxide material is experienced [16]. This sequence of events is seen in Fig. 5a where the passivation of the anode surface causes event (i) wherein the anode evolves hydrogen gas during charging instead of electrodepositing zinc. Zinc's voltage is lower than hydrogen gas evolution, and consequently the cell voltage at event (i) rises only to ~1.5 V for 20 min, after which zinc begins to plate and the cell voltage rises to 1.75 V. This failure to deposit zinc for the first 20 min causes the anode to be at a lower state-of-charge than the cathode leading to event (ii) wherein the cathode overcharges and the cell voltage hits the upper limit of 1.93 V. A few

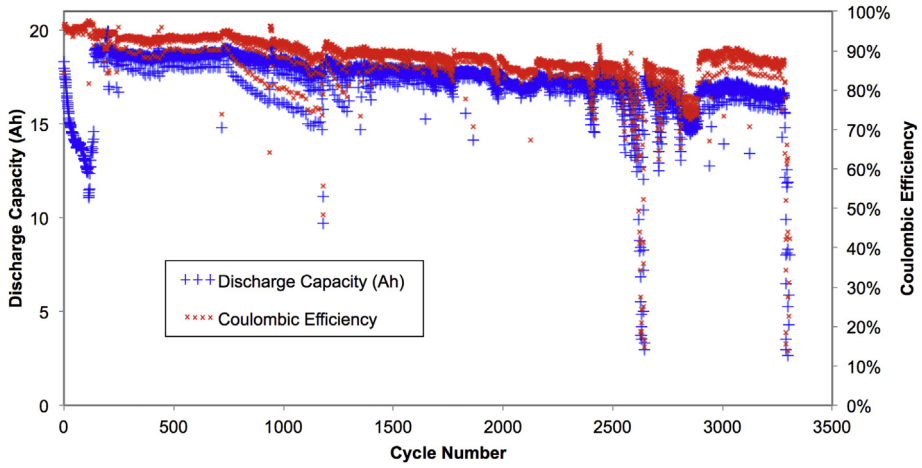

Fig. 3. Discharge capacity and coulombic efficiency of our best performing 19 Ah bench-scale cell. The sharp drops in performance occurred when the motor was accidentally cut off due to mains power outages. After flow resumed, the cells recovered.

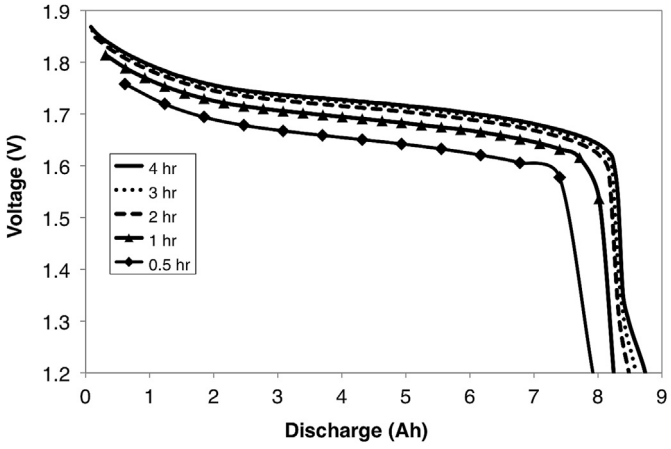

Fig. 4. Discharge capacity of the 19 Ah bench-scale cells as a function of rate of discharge.

days later with the same cell, panel b) shows the same passivation event to occur at time (iii), leading to low current charging at 1.93 V. Low current density charging forms mossy highly porous zinc morphology [8,15,17,18], which leads to short-circuits beginning at time (iv). A solution was found to avoid these short-circuits, and the cells were recovered. This passivation behavior was often seen to be connected to the anode cleaning step that immediately precedes events (i), (iii), and (iv).

The combination of the two aforementioned zinc-anode management problems eventually led to mechanical and electrochemical degradation of the sintered nickel hydroxide cathodes. As seen in Fig. 6b), an expansion of the cathodes up to 2 mm was seen with side-view photography through the transparent cell box, which is a large increase in thickness compared to undamaged (0.6 mm thick) cathodes seen in Fig. 6a). Elemental ICP-OES analysis of this black film material determined it to be roughly half nickel powder and half zinc powder. Cross-sectional electron microscopy of the cathodes showed cracking, as seen in Fig. 6d). Cracking is expected when the cathodes are overcharged. These problems led to the short cycle life of the "37KOH, 40ZnO", "45KOH, 40ZnO", and "Ni Unrestricted" cells of Table 3, and to some degree shortened the cycle life of all our tested cells. A method of avoidance of these problems is described at the end of this subsection, wherein the cycling protocol is changed, or alternatively a nickel foam is used to always keep the anode's voltage within ~300 mV of metallic zinc, which apparently prevents the anode's surface from being poisoned.

Anode surface passivation was observed to occur particularly often if its voltage was raised higher than the voltage of zinc's rest voltage in the same electrolyte, for example during the anode cleaning step it rose to ~1.5 V with respect to zinc. Five of our bench scale battery cells and four of our 555 Ah grid-scale cells were observed to experience this anode surface passivation.

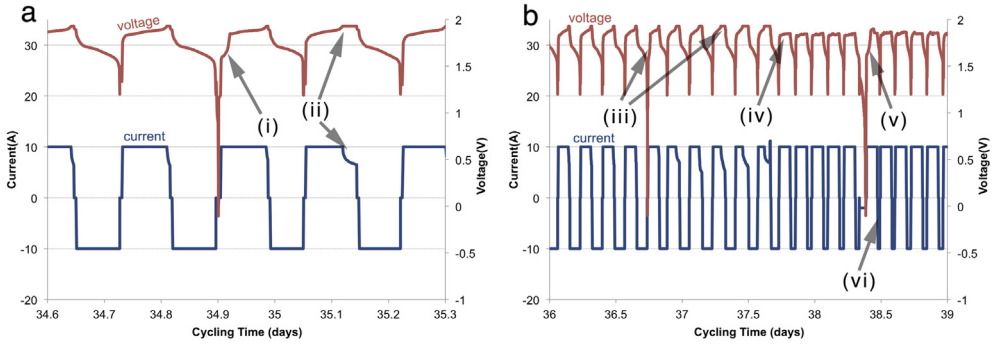

Fig. 5. Plots of cell voltage (red) and current (blue) time series. (For interpretation of the references to color in this figure legend, the reader is referred to the web version of this article).

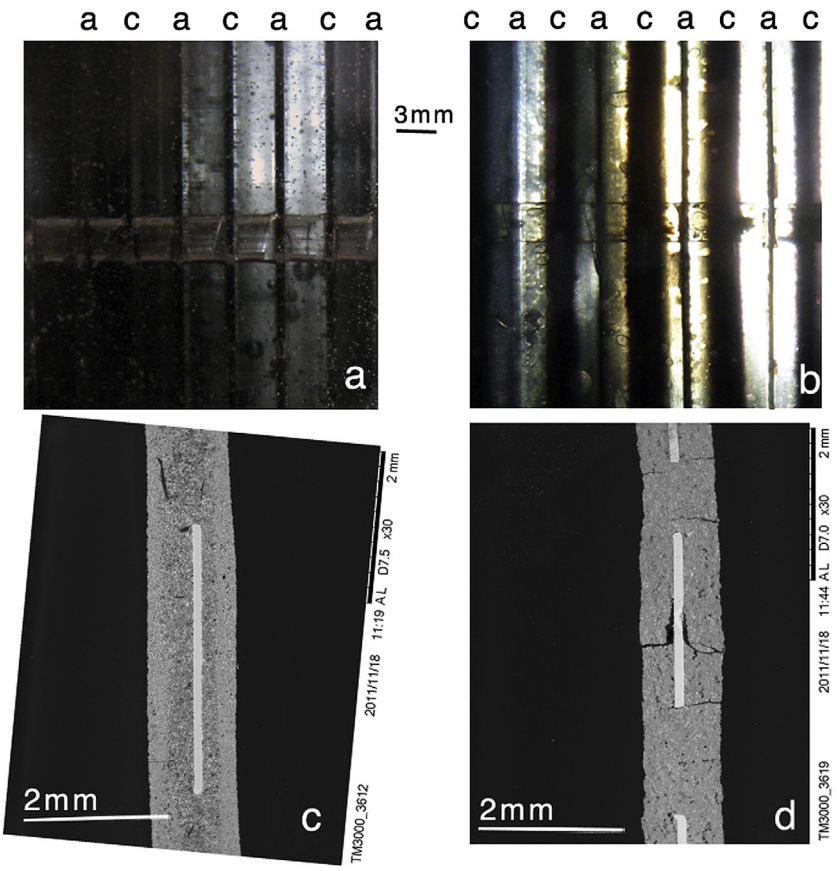

Fig. 6. Expulsion of nickel hydroxide from the sintered-nickel matrix after short-circuiting and excessive gas generation events. In a) a side-view photograph of undamaged cathodes is shown (cycled ~600 times), whereas in b) a side-view photograph of damaged cathodes is show (cycled only ~400 times). In c) and d) scanning electron microscopy show cross-sections of a new and cycled cathode respectively.

Apparently this passivation did not occur on copper anode surfaces [8], but clearly exists on the nickel surfaces studied here. We chose to use a nickel anode surface because copper dissolves into the electrolyte during the anode cleaning step, leading to fragmentation of copper and eventual failure of the mechanical strength of the anode [8]. The task of removing zinc from the anode surface is therefore an important and delicate task, wherein the anode's voltage must be raised high enough to clean off all the excess zinc but not high enough to poison the nickel surface.

A solution to this problem was found in use of a 9 × 4 cm sheet of nickel foam placed into the electrolyte. Nickel foam has high surface area and acts as a superb catalyst for electrolysis of water, therefore this nickel foam can be connected to the anode during the anode-cleaning procedure to expedite the removal of excess zinc

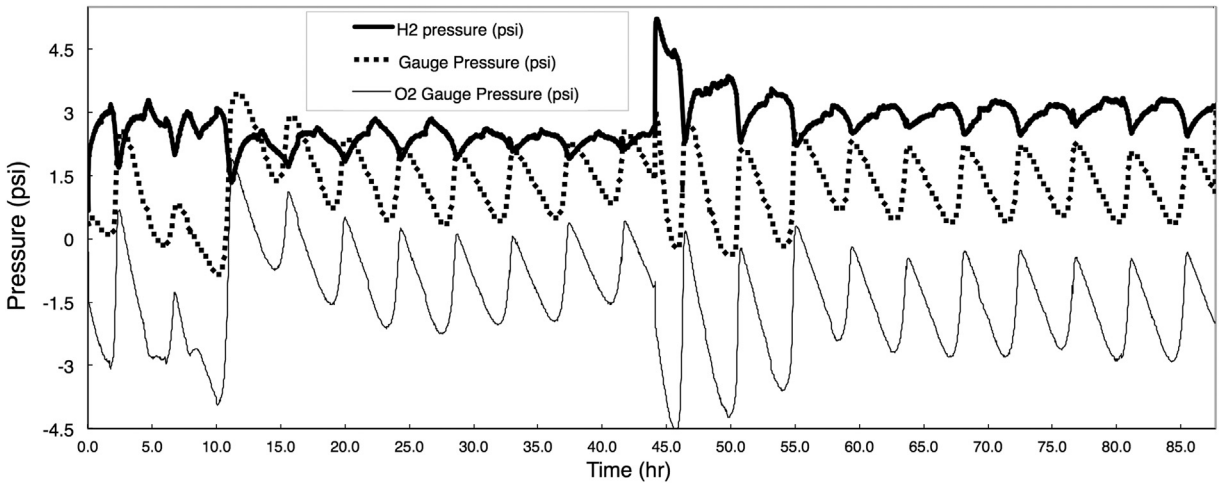

Fig. 7. Gas pressures during 21 full (100%) charge and discharge cycles are shown for a sealed-cell version of the flow-assist technology.

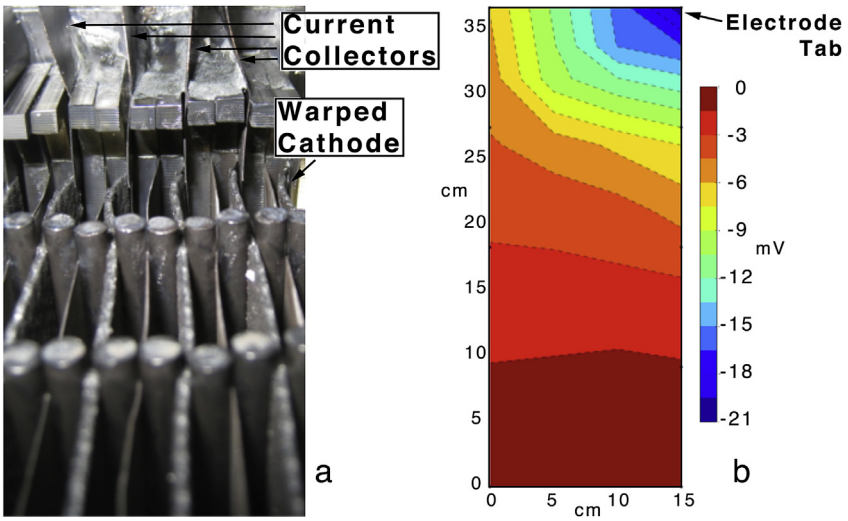

Fig. 8. a) The warping of the nickel hydroxide cathode near the tab. b) Measured electrode overvoltage (mV) during discharge at a 2 h rate.

without forcing the cell voltage to drop to −0.1 V. This nickel foam sheet may be coincidentally used for the gas management method described in Subsection 2.2, therefore the nickel foam sheet serves dual purpose. A test cell incorporating the nickel foam was built and its performance is shown in the last row of Table 3. We did not retrofit the other bench scale cells of Table 3 with the nickel foam, because they were already ∼300 cycles into testing and disassembly would be difficult. A different solution was used on them to avoid the anode-passivation problem. Their cycling procedure was changed, and in place of the −0.1 V cleaning step a 12 h rest and low-current discharge was created every tenth cycle. This 12 h rest and low-current discharge cleaned the zinc off the anodes without allowing the cells voltage to drop below ∼1.3 V, and eliminated the anode-passivation problem.

As mentioned previously, these zinc management and anode-passivation problems appeared after a few hundred cycles, at which point we made the fixes to overcome the problems and continued cycling for hundreds or thousands more cycles. See Table 3 for the final cycle life. We stopped cycling when energy efficiency dropped permanently below 75% or discharge capacity dropped permanently below 80%. The cycle life of these cells is listed in the right hand column of Table 3. The cycling of these cells continued for two years, and was marked by the above-mentioned anode-passivation and short-circuiting, by building power outages that cut power to the electrolyte-flow pumps, and occasionally by low electrolyte level (which was maintained bimonthly with fresh deionized water). The results show best performance with the cell that had 37% KOH and 60 g L^{-1} of zincate, and no difference was seen between stainless steel and nickel-coated hardware. Flow homogenizers appeared to improve performance compared to no flow homogenizers.

3.2. Performance of a sealed cell

As described in Subsection 2.2 a gas-sealed cell was tested, with no gas emissions to the environment. A nickel foam sheet was used in this cell for the dual purposes of gas pressure management and avoidance of anode-surface passivation. Fig. 7 shows data from the first twenty cycles of this cell, showing good control of headspace pressure and hydrogen concentration. Near cycle 25 the platinum recombiner catalyst became moderately poisoned and lost capacity to recombine the gases at a fast enough rate, causing the headspace pressure to rise above 5 psi and bringing the gas seal to an end. After this 25th cycle the cell was allowed to vent gas, and cycling

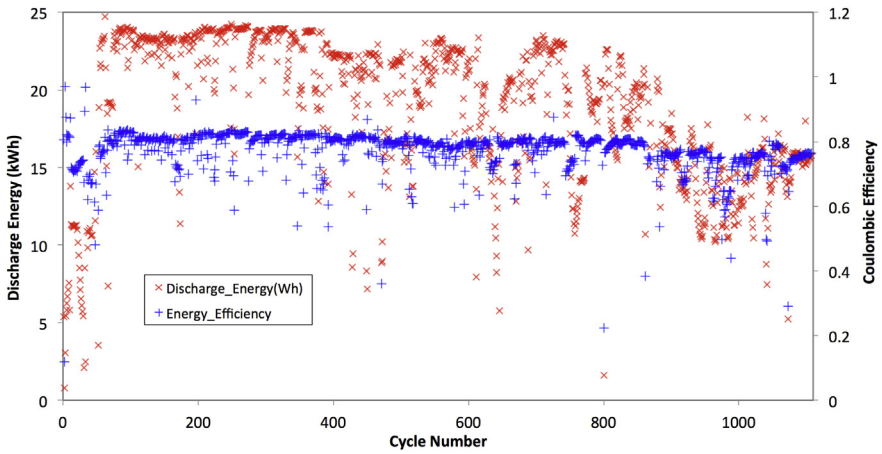

Fig. 9. Cycling performance of the grid-scale 25 kWh flow-assisted zinc-alkaline nickel-hydroxide battery.

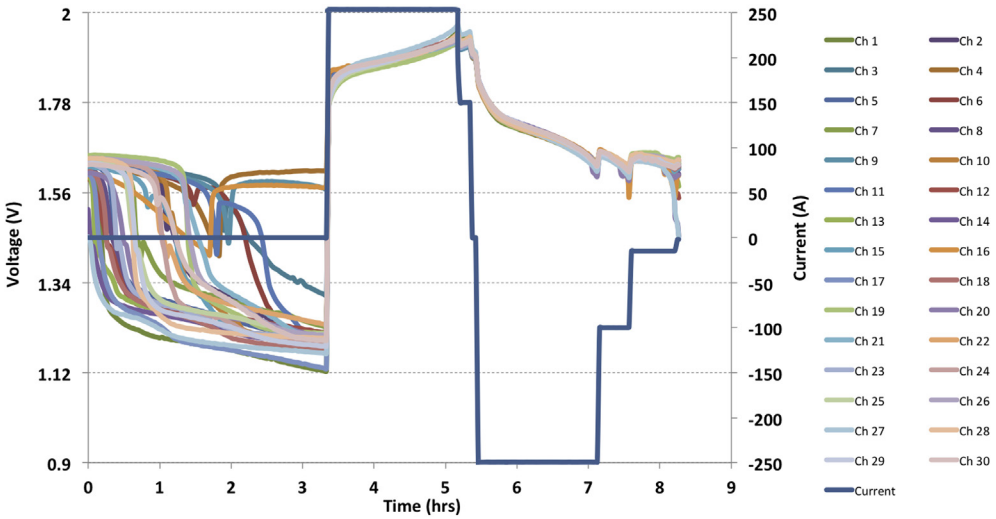

Fig. 10. Battery current and voltages for the 95th cycle, wherein the battery discharged 24,018 Wh. The voltages of all cells behave normally during this cycle. It is not necessary to see every voltage curve. The general trend is the important message.

continued with the nickel-foam being used to avoid anode-surface passivation. The final cycle life is shown in the final row of Table 3.

3.3. Grid-scale performance and failure mechanisms

Cycle testing of our 25 kWh grid-scale battery was made as described in Subsection 2.3. Individual 555 Ah cells were also cycle tested. In either case, the energy requirement for electrolyte pumping was measured to be 5 W per cell. Over a 7-h cycle this adds up to 35 Wh for pumping energy per cell. In that same seven hours the cell stored and delivered 833 Wh of energy, and therefore we find that electrolyte pumping costs only ∼4% of the energy throughput of the battery, which is not a significant concern.

One failure mechanism discovered during preliminary testing of the grid-scale electrodes was due to voltage drop in the cathodes during charge and discharge. As shown in Fig. 8a), the cathodes warped at locations within a few centimeters of the electrode's tab. To investigate this issue we welded 10 lead wires onto the perimeter of one of our cathodes in a 555 Ah cell and monitored their voltage during cycling of the cell at a two hour charge and discharge rate. Fig. 8b) shows the resulting interpolated voltage map on this cathode during the middle of a discharge, which shows that larger overvoltage is experienced by locations on the cathode within a few centimeters of the tab, meaning the nickel hydroxide in this region experienced larger volume changes than at other locations. Our discovered solution to this issue was mechanically holding and blocking the cathode sheets in this region near to the tab, to prevent this swell-shrink cycle in that region.

The 25 kWh grid-scale battery cycled for over 1000 cycles, a notable success considering it was the first grid-scale prototype of this new technology. Fig. 9 shows the cycling performance results, where it can be seen that the battery maintained energy efficiency above 80% for roughly 1000 cycles. Three cycles per day were tested, and so Fig. 9 represents a year of data. Analysis of the voltage on the individual cells shows that the decline in discharge capacity of the battery at cycles 900 and above is due to voltages of only two cells in the string. These two cells were degraded, consequently

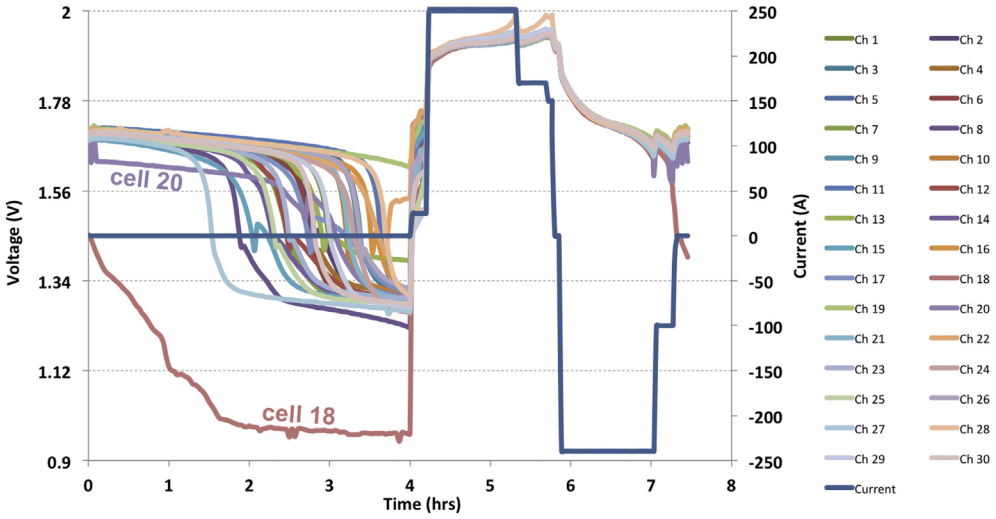

Fig. 11. Current and voltages for the 1055th cycle, for which the battery discharged only 15,716 Wh. Cells 18 and 20 behave differently than in Fig. 10 due to failure mechanisms described in the text.

Table 4
Direct materials costs for one 555 Ah cell.

Item	Cost per unit	Unit	Units needed	Item cost
Cell box	$15.00	1 box	1.0	$15.00
Rack and flow box for holding all electrodes	$10.00	1 rack	1.0	$10.00
Lid for box	$5.00	1 lid	0.3	$1.67
Pressure release valve	$2.00	1 valve	1.0	$2.00
KOH solution (37% w/w)	$0.98	1 L	20.0	$19.60
Zn powder	$4.10	1 kg	1.3	$5.33
NiOOH/graphite positive electrode:	–	–	–	–
Graphite powder	$5.50	1 kg	0.04	–
NiOOH powder	$16.00	1 kg	0.04	–
Teflon binder	$4.50	1 kg	0.005	–
Current collector and tab	$0.75	1 collector	1	–
Total for a NiOOH/graphite electrode:	$1.19	1 electrode	39.0	$63.67
Nickel-coated negative electrode sheet	$0.50	1 sheet	40.0	$20.00
Electrode spacer grill	$0.50	1 grill	78.0	$39.00
Terminal	$3.00	1 terminal	4.0	$12.00
Pump motor	$3.00	1 motor	1.0	$3.00
Shaft and impeller	$0.50	1 set	1.0	$0.50
Control electronics, wifi, wiring	$15.00	1 set	1.0	$15.00
	Total for a 555 Ah cell:			$198.23

their voltage became high too early during charge and too low during discharge, causing the entire string to stop charging and discharging prematurely.

More evidence of the passivation of the anodes, discussed in Section 3.2, was found during the setup and installation of the string. Two 555 Ah cells were accidentally cycled with their terminals reversed, leading to severe hydrogen gassing from the anodes and poor charge efficiency, <70%. These two cells never recovered, and were scrapped, but they provided important evidence that passivation arises from forcing the nickel-coated anodes to a higher voltage than normal.

Two operational problems were experienced during grid-scale battery cycling was pumping of the electrolyte. The rotating shaft driving the impeller encountered friction due to potassium carbonate growth in the hole where it penetrated the battery lid. This periodically caused the shaft to stop spinning, leading to pumping failures at a rate of roughly one failure per cell per year. Also, similar to the bench scale cells, the electrolyte level occasionally became too low. These problems caused the variation in cycling performance seen in Fig. 9. When deionized water was added to replenish the electrolyte, or the pumping shaft was freed to rotate, cycling performance immediately improved, but unknown damage to the electrodes occurred. One or two cells out of the thirty comprising the string developed poor coulombic storage capacity and triggered early ending of discharge for the entire string. Fig. 10 shows all voltages and current for the battery during an early cycle (95th), demonstrating how cell voltages behave in a healthy state. Fig. 11 shows the voltage and current for the entire battery string at

Table 5
Direct labor costs for one 555 Ah cell.

Labor process	Labor or depreciation rate	Hours needed	Labor price
Mixing electrolyte	$20.00	0.5	$10.00
Fabricating graphite/NiOOH electrodes	$20.00	4	$80.00
Stacking electrodes and spacers	$30.00	0.5	$15.00
Filling cell, sealing lid, bolting terminals	$30.00	0.5	$15.00
	Total for a 555 Ah cell:		$120.00

Table 6
Total system cost and cost per kWh.

Item	Cost	Quantity	Cost
Direct materials: 30 of the 555 Ah cells	$198.23	30	$5946.90
Direct materials: Copper bus bar, 0.5 kg	$3.00	90.0	$270.00
Direct materials: Hydrogen gas scrubber	$25.00	6.0	$150.00
Direct materials: Central logic controller	$50.00	1.0	$50.00
Direct labor: 30 of the 555 Ah cells	$120.00	–	$3600.00
Direct labor: Assembling rack, stacking batteries	$30.00	3	$90.00
Direct labor: Wiring bus bars and BMS system	$30.00	2	$60.00
	Total for 25 kWh system:		$10,166.90
	Cost per kWh:		$406.68

cycle 1055, a cycle that had a discharge energy of only 15,716 Wh. Cells 18 and 20 in this graph show degraded capacity apparent as a drop in voltage that causes discharge of the entire battery string to end before the rest of the cells are fully discharged. This behavior was consistent for cells 18 and 20 for many hundreds of cycles. During the rest (open circuit voltage) step, cell 18 has a voltage that drops much too low, indicating a lack of zinc and passivation as described in Subsection 3.1. Cell 20 shows a voltage a few tens of millivolts below nominal, indicative of a soft short-circuit, slowly draining the cathodes to the anodes.

3.4. Cost estimate for zinc-alkaline nickel hydroxide battery without separator membrane

An advantage of this battery technology is the lack of any membrane separator between the anode and cathode to control "shape change" problems with the zinc anode. A cost estimate for this battery technology is constructed using our bill of materials and labor records that we catalogued during fabrication and assembly of our 25 kWh battery, shown in Tables 4–6. Materials cost quotes were obtained from world-cheapest suppliers (such as Alibaba). The sintered nickel matrix of our cathodes is well known to be expensive. To eliminate the sintered-nickel we demonstrated in Subsection 3.1 (Table 3) a cell using graphite-paste nickel-hydroxide for the cathode that performed well for 700+ cycles. Our cost estimate makes use of this less expensive nickel cathode. Table 6 gives the total system cost for a 25 kWh battery and normalizes it by kWh, resulting in $406.68 per kWh. This cost per kWh is low enough to allow economic use of the battery in high-value grid-scale applications such as demand-charge reduction or utility-upgrade deferral. Some more work would be required to extend the cycle life of the nickel-paste cathode from 700 to1,500+ cycles.

4. Conclusions

Alkaline zinc-anode nickel-cathode batteries with flow-assist electrolyte and no separator membrane were tested at both bench scale (28 Wh) and grid scale (25 kWh). Cycle life of the grid-scale battery was demonstrated at 100% depth of discharge to be 1000+ cycles. At bench scale, cycle life of 3300 was demonstrated also at 100% depth of discharge. Typical failure mechanisms were zinc particulate short-circuiting of the electrodes and passivation of the anode's nickel surface for zinc electrodeposition. The grid-scale battery's total direct cost is projected to be near $407 per kWh. With further research and development, cycle life of 3000 to 4000 appears achievable. To achieve this improved cycling performance, further work is suggested on the effect of the anode's surface chemistry on zinc electrodeposition, on zinc growth morphology that leads to particulates and short circuiting, and demonstrating

cycle life of graphite-paste nickel hydroxide cathodes to 3000+ cycles.

Acknowledgment

This work was supported by US-DOE grant DE-EE0004224 and NYSERDA grant 18786.

References

[1] American Solar Energy Society, Tackling Climate Change in the U.S, 2007. www.ases.org/climatechange.
[2] Minnesotta Public Utilities, Final Report: 2006 Minnesota Wind Integration Study, 2008.
[3] J. Neubauer, Challenges and Opportunities for Stationary Energy Storage Markets, National Renewable Energy Laboratory, 2012, pp. 1–22. Techical Report.
[4] D.R. Walawalkar, Economics of Emerging Electric Energy Storage Technologies and Demand Response in Deregulated Electricity Markets, Carnegie Mellon University, 2008.
[5] J. Eyer, G. Corey, Energy Storage for the Electricity Grid: Benefits and Market Potential Assessment Guide (No. SAND2010-0815), Sandia National Laboratories, 2010, pp. 1–232.
[6] D. Rastler, Electricity Energy Storage Technology Options (No. 1020676), Electric Power Research Institute, 2010, pp. 1–176.
[7] Y. Ito, M. Nyce, R. Plivelich, M. Klein, S. Banerjee, J. Power Sources 196 (15) (2011) 6583–6587.
[8] Y. Ito, M. Nyce, R. Plivelich, M. Klein, D. Steingart, S. Banerjee 196(4), 2340–2345, 2011.
[9] R. Barnard, C.F. Randell, F.L. Tye, J. Appl. Electrochem. 10 (1) (1980) 109–125.
[10] L.Z. Vorkapic, D.M. Drazic, A.R. Despic, J. Electrochem. Soc. 121 (11) (1974) 1385–1392.
[12] D. Linden, T.B. Reddy (Eds.), Handbook of Batteries, third ed., 2001.
[13] V.K. Nartey, L. Binder, K. Kordesch, J. Power Sources 52 (2) (1994) 217–222.
[14] US Patent Application WO2013126839 A1, Management of gas pressure and electrode state of charge in alkaline batteries, 2013.
[15] F.R. McLarnon, E.J. Cairns, J. Electrochem. Soc. 138 (2) (1991).
[16] R.A. Huggins, Advanced Batteries, Materials Science Aspects, Springer, 2009.
[17] R.D. Naybour, J. Electrochem. Soc. 116 (4) (1969) 520.
[18] J.W. Gallaway, D. Desai, A. Gaikwad, C. Corredor, S. Banerjee, D. Steingart, J. Electrochem. Soc. 157 (12) (2010) A1279–A1286.